Journal of Energy Storage 100 (2024) 113518

Contents lists available at ScienceDirect

Journal of Energy Storage

journal homepage: www.elsevier.com/locate/est

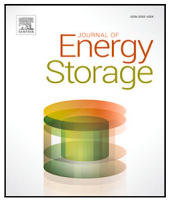

Research Papers

Analysis of the discharge process of a TES-based electricity storage system

Matteo Pecchini, Simone Peccolo, Alberto Benato *, Francesco De Vanna, Anna Stoppato

Department of Industrial Engineering, University of Padova, Padova, Italy

ARTICLE INFO

Keywords:
Renewable energy
Thermal energy storage
Off-design model
Part-load analysis
Carnot battery

ABSTRACT

Carnot battery is considered one of the most promising technologies for large-scale electricity storage. Among the available configurations, the so-called Integrated Energy Storage System (I-ESS) demonstrated its ability to compete with other large-scale storage technologies, such as pumped hydro and compressed air energy storage. However, an investigation that focusses on the performance of Brayton-based Carnot batteries under part-load conditions and adopts an off-design mathematical model is still lacking in the literature. Therefore, to predict the behaviour in part load, the characteristic curves of the turbine and compressor are included in the mathematical model of the I-ESS in conjunction with a properly tuned control system. In addition, to highlight the need to adopt off-design models of critical devices, a comparison between the developed model and various simplified models has also been performed. The results show that the average discharge efficiency of the I-ESS reaches 27%, while the maximum depth of discharge is 64%. When using simplified models, the error in the depth of discharge calculation varies from 7 to 23%. Therefore, this study highlights the crucial importance of adopting an off-design model to better predict the behaviour and performance of Brayton-based Carnot batteries without overestimating parameters such as the depth of discharge or the electricity production.

1. Introduction

Reducing CO_2 emissions from human activities is one of the most urgent challenges in our society, and the electricity sector is one of the most impactful in terms of greenhouse gas emissions. The 2023 International Energy Agency Electricity Market Report [1] states that the emissions associated with the electricity sector are approximately 13.2 Gt of CO_2. For this reason, the production of power from renewable energy sources (RES) is crucial to boost sector decarbonisation. According to the International Energy Agency [2], total additions of renewable energy capacity are increased in 2022 by approximately 13% and reached nearly 340 GW. In the next few years, an additional increase in renewable energy installations is expected due to strong and continuous policy support, as well as high electricity prices. However, variability and unpredictability, the distinctive characteristics of renewable sources, such as wind and solar, are pushing the need to develop and install energy storage units to avoid mismatches between electricity supply and demand [3].

Various energy storage technologies have been developed over the years, each with its features in terms of power, capacity, response time, etc. Among large-scale storage technologies, electrochemical (flow batteries, FBs), mechanical storage (pumped hydro storage, PHS), and compressed air energy storage (CAES) are considered the most mature and commercially available solutions. However, several problems affect these technologies, with the consequent need for new methods of storing energy and a new way of managing storage plants. In fact, FBs are characterised by a poor lifespan (5–15 years), low energy density (16–60 $\mathrm{Wh\,l^{-1}}$) and high investment costs (120–1000 $\mathrm{\$\,kWh^{-1}}$) [4–6]; PHS presents low energy density (0.5–1.5 $\mathrm{Wh\,l^{-1}}$) and high installation costs (600–2000 $\mathrm{\$\,kWh^{-1}}$). Moreover, this technology requires an almost constant mass flow rate and stringent morphological constraints. The large exploitation of suitable PHS installation sites (especially in Europe and the United States), coupled with the drawbacks mentioned above, limits the further spread of this mature technology [6–10]. CAES suffers from similar problems, such as high investment costs (40–200 $\mathrm{\$\,kWh^{-1}}$), low energy density (3–12 $\mathrm{Wh\,l^{-1}}$) and geographical constrains; in addition, this technology often requires a fossil fuel stream [6,11,12]. All these aspects represent important limits that preclude a wide and fast development of such technologies and require finding new solutions for electricity energy storage, able to mitigate the unpredictable behaviour of variable and intermittent renewable sources and to meet the geographical needs. As a consequence, in recent years, researchers have begun to look at *thermo-mechanical* storage technologies. Among them, we can find the so-called *Carnot batteries* (CBs), one of the most promising solutions in the field of large-scale electricity storage, as underlined by Vecchi et al. [13] and Lampasi et al. [14]. The general working principle of a CB is as follows: during the charge, electricity is converted into heat and stored as thermal

* Corresponding author.
E-mail address: alberto.benato@unipd.it (A. Benato).

https://doi.org/10.1016/j.est.2024.113518
Received 30 November 2023; Received in revised form 17 August 2024; Accepted 23 August 2024
Available online 4 September 2024

energy. When power is requested, thermal energy is converted back into electricity and delivered to the grid.

Several types of CB have been studied over the years (i) using sensible and latent thermal energy storage (TES), (ii) performing the charge by direct electric heating, heat pumps and low temperature waste heat, and (iii) discharging the system by means of different thermodynamic cycles such as the Rankine, Brayton–Joule, and Kalina cycles [15]. Despite the various solutions proposed, the most studied CB plant arrangement is the one named Pumped Thermal Energy Storage (PTES). PTES is characterised by a high energy density, a low self-discharge rate, no geographical limitations, and a small installation footprint. It is based on a high temperature heat pump cycle, which converts the off-peak electricity into thermal energy and stores it inside two man-made thermally isolated tanks (usually called *Thermal Energy Storage* or *TES*): one hot, with a storing temperature from 500 °C to 1000 °C, and one cold, characterised by a storing temperature ranging from −150 °C to −70 °C. During high-demand hours, the system is discharged: in this phase, a thermal engine cycle is adopted to convert stored thermal energy into electricity. The working fluid is a gaseous medium, air or argon, while electricity is stored as sensible heat using inexpensive and solid materials such as concrete, gravel, or other common minerals [16–18]. In addition, PTES allows the use of components from existing out-of-market fossil-based thermal power plants. The latter is the motivation that led the authors of this work to develop the Integrated Energy Storage System (I-ESS): a storage unit that can be embedded in unused or currently being decommissioned fossil-based power plants, as well as at the same installation site for wind and solar plants [19,20]. This system is described in depth in Section 2, but can be seen basically as a modified gas turbine in which the combustion chamber is replaced by a sensible TES. Compared to PHS and CAES, I-ESS does not suffer from geographical constraints and does not require a stable water flow, such as PHS, or a natural gas stream such as CAES. Unlike FBs, the I-ESS plant is characterised by a longer cycle life, whereas, compared to PTES, the I-ESS layout features a lower complexity.

Previous studies have demonstrated the feasibility of the I-ESS plant (see, for example, [19,20]) and its ability to integrate with variable renewable facilities, to mitigate its variable behaviour (as highlighted in [21–23]). However, it is imperative to investigate in the proper way the off-design and dynamic behaviours of the system, specifically during the discharge phase. In fact, in the literature, only a few authors have investigated this field, such as Frate et al. [24,25], while most of the work focusses primarily on the design of the system using simplified models (for example, [26–28]). The I-ESS system works most of the time in off-design conditions, since the temperature of the storage changes continuously, in particular during the discharging phase. In addition, the needs of the electrical grid often require the operation of the I-ESS in partial load conditions. These two aspects explains the importance of an off-design analysis. To this end, in this work the mathematical model of the I-ESS is improved by implementing the performance maps of the turbomachinery and a custom control strategy in order to make the mathematical model capable of predicting the off-design behaviour of the I-ESS during discharge, given its particular importance. To highlight the importance of a precise modelling of the part-load behaviour of the system, this comprehensive off-design model is subsequently compared to different simplified models from the literature [20,21,29–31].

The rest of the work is organised as follows. Section 2 describes the layout of the I-ESS, while Section 3 presents a detailed description of the off-design mathematical model of the I-ESS storage unit, while Section 4 presents the case study under investigation. Section 5 summarises the most interesting results of the numerical investigation, while Section 6 states the conclusions.

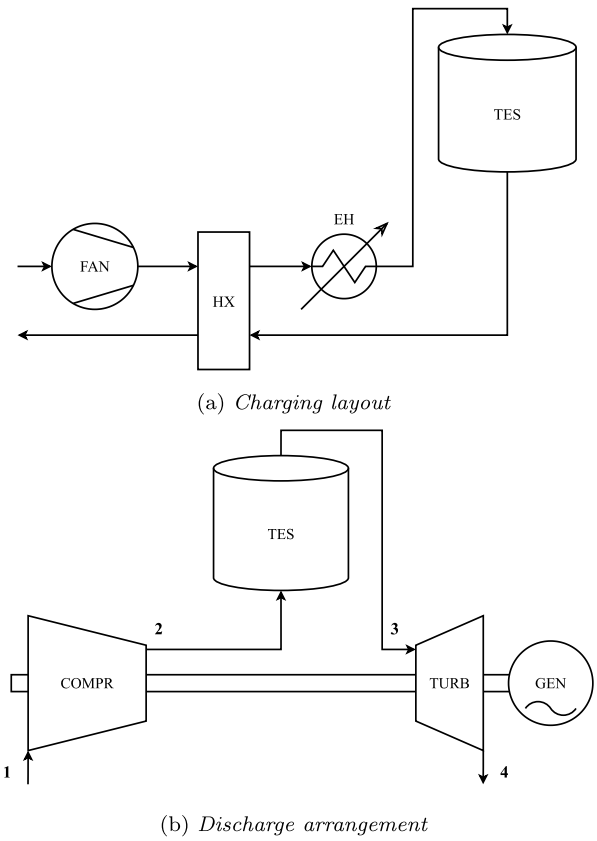

Fig. 1. Layout of the I-ESS system in (a) charge and (b) discharge modes.

2. Integrated Electricity Storage System (I-ESS)

The storage plant considered in this work is based on the configuration developed, patented and tested by Benato et al. [19,20]. The arrangement is named the “Integrated Energy Storage System” (I-ESS) and consists of a thermo-mechanical unit for storing electricity in the form of sensible heat that allows the use of components of existing unused or in-decommissioning fossil-based power plants. In this way, the system provides flexibility to the grid without installing additional capacity. The layout of the plant is sketched in Fig. 1.

In this configuration, air is the heat transfer fluid and, during the charging phase, a fan guarantees its circulation in the circuit. After being sucked, the air is preheated in a heat exchanger (HX) using the energy content of the air leaving the storage tank and then heated up by an electric heater (EH). At this point, the air is characterised by a high temperature and enters the TES tank, where it heats up the solid material that makes up the storage tank: thus, electricity is stored as sensible heat. The adoption of the EH allows to maintain the air temperature at the inlet of the storage tank at a fixed value, independently of the other operating conditions.

During the discharging phase, the system follows a Brayton–Joule thermodynamic cycle: the arrangement is similar to that of a gas turbine, but the combustion chamber is replaced by the storage tank. Consequently, the storage medium that was previously heated during the charging phase can release its energy by increasing the air temperature. In more detail, air under ambient conditions is sucked and compressed by a compressor. Then it is heated in the TES: the temperature of the storage material progressively decreases as the discharge proceeds. Finally, air at high pressure and temperature expands through a turbine and is released into the atmosphere. The mechanical power generated by the turbine is converted into electricity through the electric generator. In the I-ESS configuration, the compressor and the

turbine can be radial or axial turbomachines, depending on the plant nameplate power.

Basically, this technology allows us to store the excess of electricity generated by renewable sources as sensible heat and to inject it into the grid in a second moment, during the discharging process, starting from the heat previously stored in the TES tank.

Previous studies have shown that, despite poor efficiency, the plant is feasible and the investment costs to build an I-ESS are low. So, I-ESS can compete with other ES technologies [19]. Furthermore, a proper selection of the type and shape of solid storage material allows the plant to reduce costs, as well as design a storage facility that can store a different amount of energy in the same volume [20]. A feature that intrinsically guarantees the scalability of the plant based on the needs of the network. However, an in-depth analysis of plant behaviour under off-design conditions is still lacking. In previous works carried out by the authors on the I-ESS, a simplified mathematical model was used, which does not take into account the operating ranges of the turbomachinery and the variability of their performance under different working conditions [20–23]. To fully understand the potential of the proposed storage system and develop custom management strategies, the decrease in turbomachinery efficiency under part-load conditions must be taken into account. For these reasons, this work is focused on off-design modelling of the I-ESS system with an in-depth description of the compressor and the turbine through the use of performance maps. Although the layout of both working conditions is shown in Fig. 1, in this work only the discharge phase is investigated. The reason for this choice is that in the charge system as it is, the fan works in stationary conditions independently on the state of charge of the TES, and so a simplified constant parameter model is accurate enough to predict the performance of the charge system.

3. The I-ESS off-design numerical model

During the delivery phase, the thermal reservoir temperature profile changes continuously. This means that the turbine inlet temperature (TIT), which is the driving parameter in calculating the equilibrium point of the discharge system, also changes continuously. This fact leads to important consequences: unlike a conventional power plant, the I-ESS never works under design conditions. Therefore, it is important to build a mathematical model able to predict its off-design behaviour. Moreover, the system operates in a continuous transient state, and consequently the steady-state working point does not exist.

In the mathematical model proposed in this work, only the thermal reservoir is analysed as dynamic, whereas the rest of the components, as well as the control strategy, are treated with a steady-state approach. This means that the model is built considering that the time constant of the thermal phenomena is higher than the time constant of the mechanical one. With this approach, a pseudo-steady-state equilibrium point is computed at each time step. Obviously, this way of modelling the turbomachinery is widely adopted and guarantees to describe in an appropriate manner the behaviour of the system, especially if the simulation time involves several hours. However, to predict the step response and the start-up/shut-down of the storage unit, a proper dynamic model of the whole system must be built, but this is beyond the objectives of this work.

The system consists of two axial turbomachines and a packed-bed thermal reservoir. The power regulation of the plant is performed by acting on the angle of the variable inlet guide vanes (VIGV) at the compressor inlet, while the rotational speed of the shaft remains constant. The model is built in a MatLab environment, while the thermophysical properties of both air and storage material are derived from the *NIST* databases.

3.1. Compressor model

Turbomachinery is modelled with a zero-dimensional approach. In fact, the behaviour of both the compressor and the turbine is described through their performance maps. Standard maps are taken from the commercial software database [32] and scaled according to the point of design. For the compressor, the working point, which is characterised by a certain combination of pressure ratio (pr), mass flow rate ($\dot{m}$) and isentropic efficiency (η_{is}), is expressed as a function of rotational speed (N) and the auxiliary coordinate β (see Eq. (1)).

$$\{pr, \dot{m}, \eta_{is}\}_c = f(\beta_c, N_c) \tag{1}$$

Through interpolation of the maps, these values can be derived. Then, providing as input the inlet pressure and temperature, it is possible to evaluate the outlet conditions using Eqs. (2) and (3).

$$p_2 = p_1 \cdot pr_c \tag{2}$$

$$T_2 = T_1 \cdot \left(1 + \frac{1}{\eta_{is,c}} \cdot \left(pr_c^{\frac{\gamma-1}{\gamma}} - 1\right)\right) \tag{3}$$

During off-design operating conditions, the I-ESS management system varies the VIGV angle (α_{IGV}) to keep the rotational speed constant. The correlations that describe the modification of the compressor working point as a function of α_{IGV} are as follows.

$$a_{VIGV} = \frac{\partial \dot{m}\ [\%]}{\partial VIGV\ [^\circ]} \tag{4}$$

$$b_{VIGV} = \frac{\partial (pr_c - 1)\ [\%]}{\partial VIGV\ [^\circ]} \tag{5}$$

$$c_{VIGV} = \frac{\partial \eta_{is}\ [\%]}{\partial VIGV\ [^\circ]} \tag{6}$$

The values of the coefficients a, b, and c are set equal to 1, 1 and 0.01 as suggested in Ref. [33]. The positive values of α_{IGV} correspond to the closure of the variable inlet guide vanes, while negative values mean an opening of the VIGVs with respect to the design position ($\alpha_{IGV,des} = 0$). The range of variation α_{IGV} was set considering a typical range of VIGVs angles (from −5 to +40) [33,34].

3.2. Turbine model

The turbine is modelled using standard maps scaled according to the design values of the pressure ratio and the corrected mass flow, similarly to the compressor case. In fact, as given for the compressor, the values of the mass flow rate, the pressure ratio, and the isentropic efficiency are expressed as a function of the rotational speed and the auxiliary coordinate β (Eq. (7)).

$$\{pr, \dot{m}, \eta_{is}\}_t = f(\beta_t, N_t) \tag{7}$$

The turbine geometry is fixed and there are no variable inlet guide vanes. Thus, the outlet temperature and pressure are calculated according to Eqs. (8) and (9).

$$p_4 = \frac{p_3}{pr_t} \tag{8}$$

$$T_4 = T_3 \cdot \left(1 - \eta_{is,t}\left(1 - \left(\frac{1}{pr_t}\right)^{\frac{\gamma-1}{\gamma}}\right)\right) \tag{9}$$

3.3. Thermal energy storage model

The thermal energy storage tank is the key component of the I-ESS plant. Several models can be found in the literature for the description of the thermal reservoir [35] but, in this case, the TES-PD model developed by Benato et al. [26] is adopted. The TES-PD model is a 1D model in which the tank is discretised into n layers characterised by the same dimension. The influence of the number of discretisations, on both the computation time and the accuracy in the calculation of the temperature profile, has been thoroughly investigated in Ref. [26]. One of the peculiarities of this model is its ability to take into account the

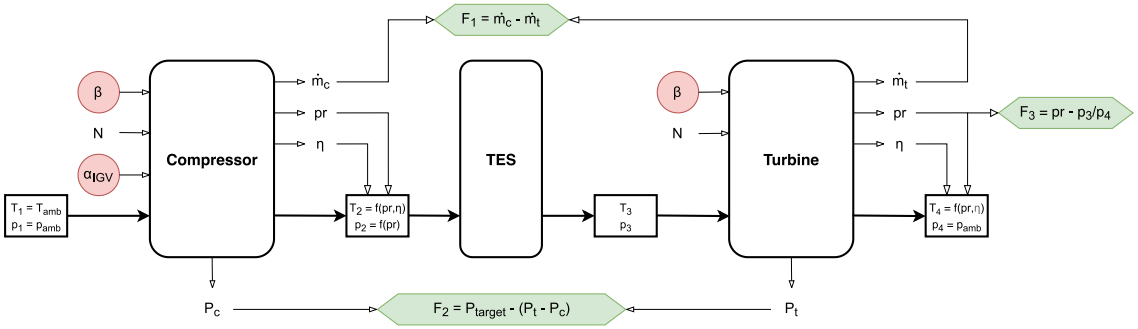

Fig. 2. Scheme of the calculation for the matching procedure. The matching variables are highlighted in red, while the functions are highlighted in green. (For interpretation of the references to colour in this figure legend, the reader is referred to the web version of this article.)

variability of the thermophysical properties of both the solid storage material and the heat transfer fluid. For more details, the interested reader can refer to [26].

3.4. Components matching

The I-ESS model calculates pseudo-steady-state points, where the turbomachines are supposed to instantaneously adapt to the thermal behaviour of the reservoir. Accordingly, for each time step, the power and the mass balance are fulfilled. In this optics, finding the equilibrium point of the system requires solving a system of non-linear equations of dimension three [36]. In the case under analysis, the procedure is based on the gradient-based `fsolve` algorithm available in the *Matlab* suite. The algorithm employs a variant of the Powell method (trust-region algorithm [37]). In Eq. (10), which describes the algorithm, δx is the vector that contains the step changes of the matching variables, J is the Jacobian matrix and F is the vector with errors. The matching variables are β_{compr}, α_{IGV} and β_{turb}, while the errors come from the check of the turbine pressure ratio, the mass continuity, and the power balance, as shown in Fig. 2.

$$J \cdot \delta x = -F \tag{10}$$

At each iteration k, the new variables are calculated as $x_k = x_{k-1} + \delta x$. The system is solved when $F = 0$. The final values of β_{compr}, α_{IGV}, and β_{turb} are those that meet the equations of mass and power balance and give a net power equal to that set as input.

4. Case study

The purpose of this work is to study the off-design behaviour of the I-ESS system during the discharge process, to improve the accuracy of the plant behaviour prediction. As a consequence, the design parameter of the system must be introduced. The I-ESS design parameters are the same as those in the work presented in Ref. [21] to allow for a proper comparison of the results between using the off-design model and the simplified model.

In particular, the thermal storage volume is set equal to 250 m^3, while its height is 6.6 m. The packed bed is made up of spheres of aluminium oxide (Al_2O_3). The density, void fraction, and diameter of the spheres are reported in Table 1, as well as the other main characteristic parameters.

The design power of the plant is set at 0.8 MW, while the design compressor pressure ratio and the polytropic efficiency of both turbomachines are set at 8.5 and 0.85, respectively. In the case under analysis, both the compressor and the turbine have an axial configuration and the rotational speed is constant. Based on the design characteristics of the gas turbine used to build the I-ESS power train, the thermal reservoir design temperature, which is equal to the turbine inlet temperature, is set at 1200 K while the air mass flow during discharge is assumed to be equal to 3.9 kg s^{-1}. As we have previously seen, the turbomachines have an axial arrangement; therefore, for the compressor and the turbine, an axial map is selected from the commercial software database. Subsequently, the selected maps are scaled according to the design values. Note that this is common practise in the case of a lack of information on the performance maps of the machines considered [33,38,39].

Table 1
Design characteristics of the TES.

Geometry	Packed-bed	
Material	Al_2O_3 (aluminium oxide)	
Elements' shape	Sphere	
TES volume	250	m^3
TES height	6.6	m
Al_2O_3 density	3990	kg m^{-3}
Void fraction	0.4	–
Spheres diameter	50	mm

To properly study the delivery phase, the discharge investigation is carried out starting from a TES tank under isothermal conditions (1200 K).

5. Results and discussion

5.1. Off-design performance of the I-ESS

After model validation (see, e.g., [19,20]), a preliminary investigation is conducted with the aim of finding the technical minimum of the system. As previously said, for simplicity, the reservoir is considered, at the beginning of the simulation, in an isothermal condition. At the beginning of the discharge phase, the I-ESS deliverable power is set equal to the nameplate one. However, with the progress of the discharge, the temperature of the packed bed decreases and, consequently, the turbine inlet temperature decreases too. Therefore, the I-ESS management system is not able to maintain both the power and the rotation speed at the design values. Therefore, since the control strategy is devoted to maintaining a constant rotational speed, the power delivered to the grid is reduced (see Fig. 3a). The power reduction continues until the system can no longer provide power by maintaining a constant rotational speed. This condition corresponds to a power equal to about 40% of the design one. Taking into account the safety margin, the I-ESS technical minimum is set equal to 50% of the gas turbine nameplate power.

The analysis of the discharge phase from the full charge to the technical minimum reveals that, as the TIT changes, the equilibrium point of the system also changes. Therefore, to maintain the rotational speed constant, the angle of the VIGVs must be continuously adjusted (Fig. 3b). The initial value of α_{IGV}, when the VIGVs are in the design condition, is $\alpha_{IGV} = 0$. Initially, to maintain the rated power, the VIGVs have to slightly open to counterbalance the decrease in the TIT. Then, when α_{IGV} reaches its lower minimum of −5, the power is scaled and

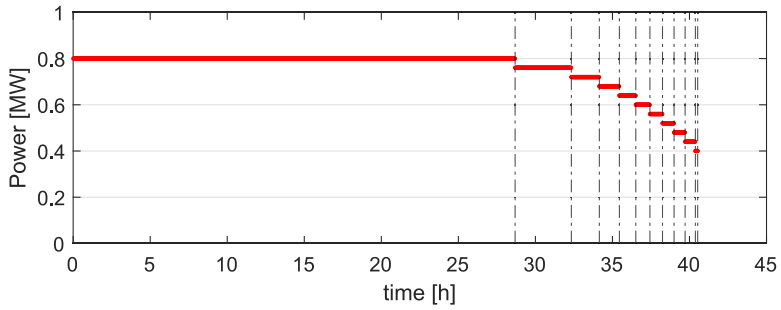

(a) *Power trend over time during discharge phase.*

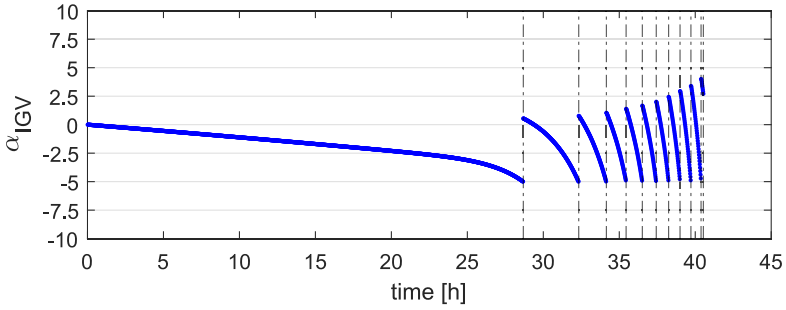

(b) *VIGV angle trend over time during discharge phase.*

Fig. 3. Regulation of the VIGV according to the power level.

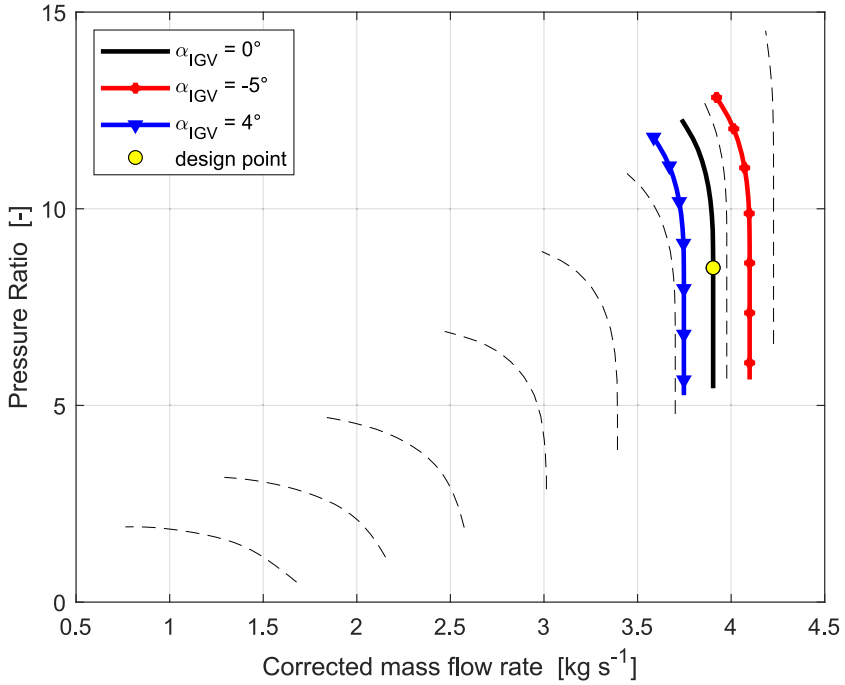

Fig. 4. Shift of the speedline according to α_{IGV}. The red and the blue lines correspond to the minimum and the maximum values assumed by α_{IGV} during the discharge, respectively. (For interpretation of the references to colour in this figure legend, the reader is referred to the web version of this article.)

α_{IGV} suddenly increases to a positive value. Fig. 4 shows the shape of the compressor map for the minimum (red line) and the maximum (blue line) values of α_{IGV} during discharge.

As said, during the delivery phase, the temperature of the packed bed decreases. Fig. 5 shows the temperature trend of some layers over time. It is interesting to note that the temperature of the first layers quickly drops to 600 K, which is equal to the compressor outlet temperature. The first layer is slightly heated after some time step, and this is due to an increase in the compressor pressure ratio related to the regulation of α_{IGV}. The discontinuities in the temperature trend derive from the step regulation of the net power, as shown in Fig. 3. The graph in Fig. 5 also shows the trend of TIT over time: it follows the trend of the last layers of the reservoir.

Fig. 6 shows the thermodynamic cycle at the beginning and end of the discharge process: at the end of the discharge, both $\eta_{is,c}$ and TIT are lower compared to the design point.

The number of layers in which the packed bed is discretised affects both the accuracy of the calculation and the simulation time. However, the focus of this work is to study the performance of the whole system, rather than the thermal storage itself. Therefore, a sensitivity analysis

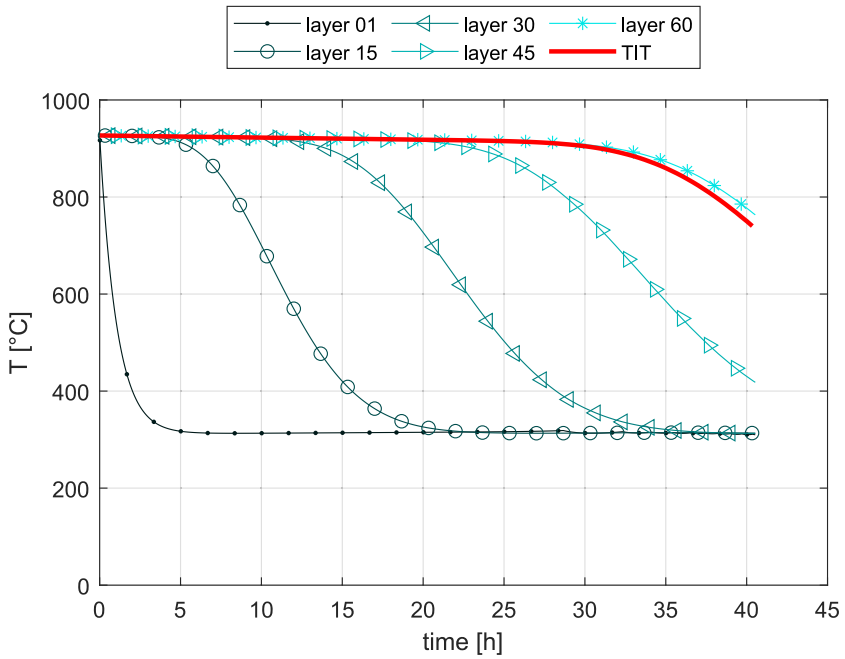

Fig. 5. Temperature trend of some sample layers and TIT trend over time.

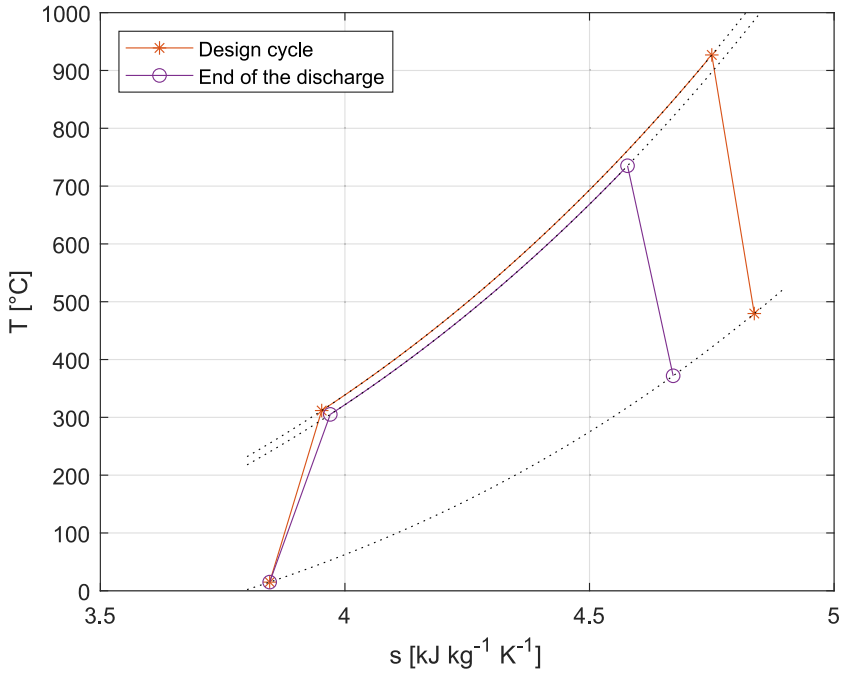

Fig. 6. Thermodynamic cycle at the design point and at the end of the discharge.

is performed to evaluate the effect of the number of layers (n) on the accuracy of the model.

The turbine inlet temperature is selected as a key parameter as the driving variable in the calculation of the thermodynamic cycle. The analysis revealed that, varying n from 30 to 160 with a step of 30, the standard deviation in the TIT calculation at the end of discharge is approximately 0.02%. For this reason, a number of 60 layers is chosen as a good compromise between computational speed and accuracy.

After this preliminary investigation devoted to the definition of the technical minimum and the number of layers for the discretisation, it is interesting to study the discharge time of the system. Two performance parameters can be defined: the total discharge time, and the discharge time at nameplate power, corresponding to the maximum amount of hours for which the system can provide the design power. The TES temperature was adjusted to explore the effects of both of these parameters. The results of the simulations are presented in Fig. 7, which shows the influence of the temperature at which the heat is stored on the discharge time. For these calculations, the design power is set to 0.8 MW, while the power step size is 5%. As we can see, the total discharge time is strongly influenced by the reservoir design temperature: increasing $T_{TES,design}$ from 1100 K to 1300 K the total discharge time increases from 32.4 h to 48.6 h (+50%). The storage temperature also determines the discharge time at nameplate power. Varying the TES temperatures from 1100 K to 1300 K, we observe an

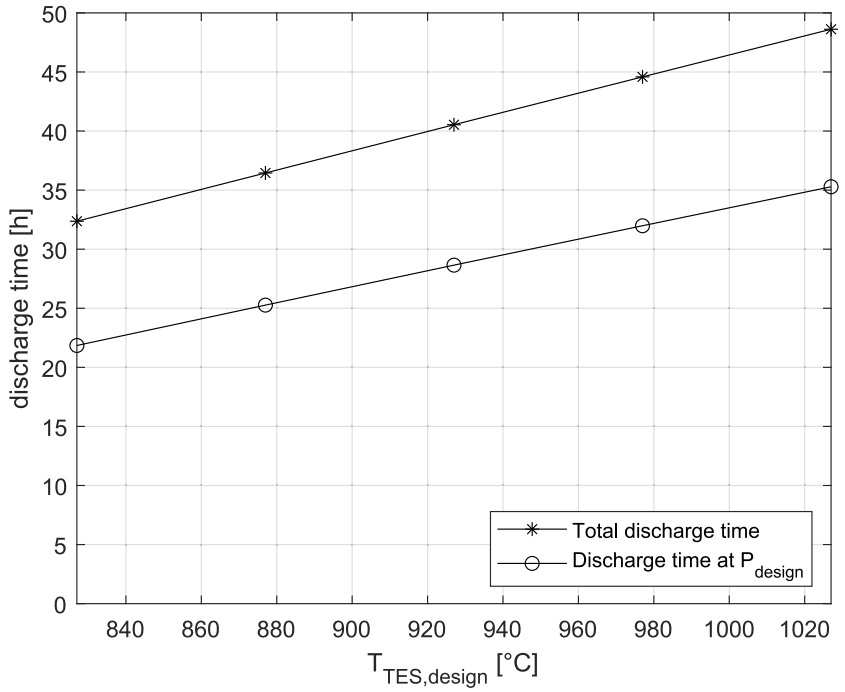

Fig. 7. Influence of the storage temperature on the discharge time.

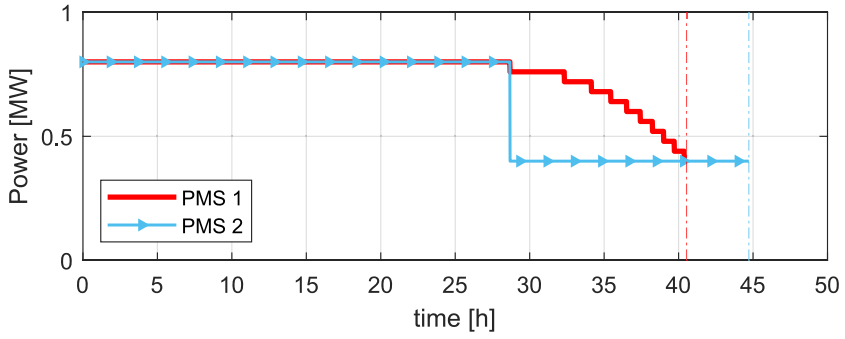

Fig. 8. Influence of the power decline step on the discharge time.

increase by 61% of the discharge time. Moreover, the efficiency of the Brayton cycle is strongly influenced by TIT. Hence, having a high $T_{TES,design}$ is beneficial for the discharge phase.

The off-design model established that the system cannot provide the nameplate power for the entire discharge time: due to continuous decrease of TIT, the power must evolve consequently. At certain point of the discharge phase, the power has to be reduced to maintain the rotational speed constant. The strategy by which the power reduction is managed affects the discharge duration. Fig. 8 shows the difference between two different power management strategies (PMSs). PMS 1 involves a gradual reduction of the power with 5% steps. On the other hand, PMS 2 consists on a sudden drop of the power towards the technical minimum. The results show that managing the system with PMS 2 (light blue line in Fig. 8) allows to extend the discharge time by 4.2 h. This comes from the fact that part of the "available power" is unused. The choice of the management strategy may depend on economic evaluations and on the requests of the grid operator.

The off-design model allows for the determination of the maximum depth of discharge of the TES. To do so, the maximum thermal energy that can be stored in the tank must be calculated. With the hypothesis of heating the tank from ambient temperature (293 K) to 1200 K, the maximum storable thermal energy is 169 MWh_{th}. Taking into account the full discharge, the maximum exploitable thermal energy can be calculated as in Eq. (11).

$$E_{th,discharge} = M \cdot \frac{1}{n} \cdot \sum_{j=1:n} \left(\int c_p(T) \cdot dT \right) \tag{11}$$

where n is the number of layers, M is the mass of the solid and c_p is the specific heat of the solid. Fixing the technical minimum at 50%, the maximum exploitable thermal energy is 108 MWh_{th}. Therefore, the depth of discharge is about 64%.

The electrical energy produced during a complete discharge process results in 31 MWh_{el}. Note that for the hypothesis of the investigation performed, the charge phase is not modelled. Therefore, the Round-Trip Efficiency (RTE) cannot be defined on the basis of the selected starting state of charge. However, considering the TES as isothermal at a temperature of 1200 K, the efficiency of the discharge phase can be computed as in Eq. (12), and resulted equal to 27%

$$\eta_{discharge} = \frac{E_{el,discharge}}{E_{th,discharge}} \tag{12}$$

This has to be considered as an average value. During discharge, in fact, as the TES cools down the TIT decreases, and so does the efficiency of the Brayton–Joule cycle. Fig. 9 shows the trend of the efficiency of the discharge system as a function of the state of charge of the system. For a large part of the process, η_d remains constant to

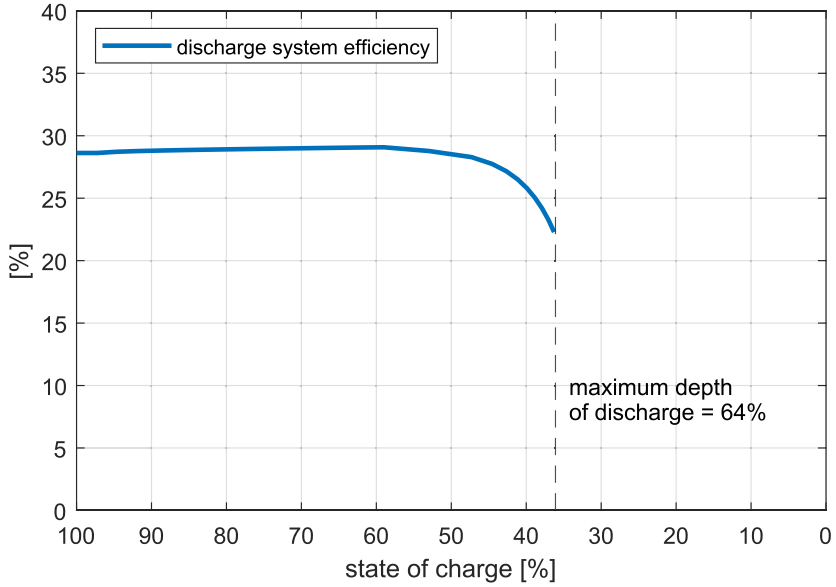

Fig. 9. Efficiency of the discharge system as function of the state of charge of the TES.

its maximum value (29%) because the TIT is nearly constant. Around a state of charge of 50%, η_d starts to decrease as a consequence of the reduction of TIT. At the end of discharge, the efficiency of the system is 22%, substantially lower than the average value of 27%. This gives an important general indication. Since the efficiency of Brayton-based Carnot batteries is sensitive to TIT, it is recommended not to reach the maximum depth of discharge of the TES, as it would lead to low values of efficiency.

5.2. Comparison between the comprehensive off-design model proposed in this work and simplified models form literature

The results presented in Section 5.1 (obtained with the off-design model presented in this work) are compared to those obtained using different simplified models from the literature. Three representative simplified approaches were selected to simulate the discharge of a Brayton-based Carnot battery, and all are based on a *constant compression ratio* approach [31]. To allow for a consistent comparison, these models are used setting the same design variables reported in Section 4, and applying boundary conditions as briefly explained in the following:

- Simplified model 1 (SM1): it is the model used by the authors in previous studies on the I-ESS [20–23]. The compression ratio and the power generated are kept constant, while the air mass flow rate is variable. During discharge, $\dot{m}_{air}$ increases to overcome the decrease in TIT. Characteristics maps and VIGVs are not included in the model. However, an operating range for the compressor is established, setting an upper limit on the mass flow rate equal to $1.05 \cdot \dot{m}_{air,design}$. The discharge stops when $\dot{m}_{air}$ reaches this limit.
- Simplified model 2 (SM2): It is similar to SM1 (constant pressure ratio and constant power), but $\dot{m}_{air}$, is free to vary without limits, and the discharge time is fixed priorly, as done in several works in the literature. The discharge time is set equal to that calculated with the comprehensive off-design model presented in this work.
- Simplified model 3 (SM3): in this case, the compression ratio and $\dot{m}_{air}$ are constant during discharge, while the power is variable. In this model, the delivery phase stops when the TES is completely discharged [29,30]. Therefore, the discharge phase lasts until the system can deliver positive power.

Fig. 10 shows the difference in the state of charge at the end of discharge using different mathematical models. It can be seen that with the simplified model used by the authors in previous studies on the I-ESS (SM1), the charge stops earlier because $\dot{m}_{air}$ rapidly reaches the upper limit set for the turbomachinery. On the other hand, SM3 leads to an almost isothermal temperature profile inside TES around 300 °C, which is the compressor outlet temperature. For SM2, the final state of charge of TES is lower because, even if the discharge duration is the same as that obtained with the comprehensive off-design model, $\dot{m}_{air}$ has no limits and reaches really high values during discharge to overcome the decrease in TIT.

From the final state of charge of the TES it was possible to evaluate the maximum depth of discharge with the different simplified models, as well as the electricity produced during a complete delivery phase, and the discharge efficiency. The results are shown in Fig. 11. The error in the calculation of discharge efficiency is approximately 1% for all simplified models, compared to the model described in Section 3. However, the discrepancy in evaluating the depth of discharge is huge. SM1 displays the maximum error; in fact, this model underestimates the maximum depth of discharge by 23%, which means 15 percentage points (49% instead of 64$). SM2 and SM3, on the contrary, overestimate it by 7% and 11%, respectively (4 and 7 percentage points). The total electricity production calculated with the model presented in this work results in 31 MWh; using simplified models SM1, SM2 and SM3 the error is −22%, +6% and +8%, respectively.

Therefore, simplified models are accurate enough to be used to evaluate the efficiency of the system. However, comprehensive off-design models are fundamental for the calculation of the discharge duration, the electricity production, and the depth of discharge of the storage system. In particular, we can conclude that the simplified model used by the authors in previous works on the system under investigation (SM1) was not accurate enough to predict the off-design performance of the I-ESS. However, the simplified model was built to perform year-long simulations in working conditions close to the design point and not to provide a detailed description of the part-load behaviour of the system [21]. For this reason, computational speed was considered more important than accuracy. In fact, the detailed off-design model takes about 10 times the computational time per minute of simulation compared to the simplified model.

6. Conclusions

In this study, the off-design performance of an integrated power storage system has been analysed. To this end, a proper off-design

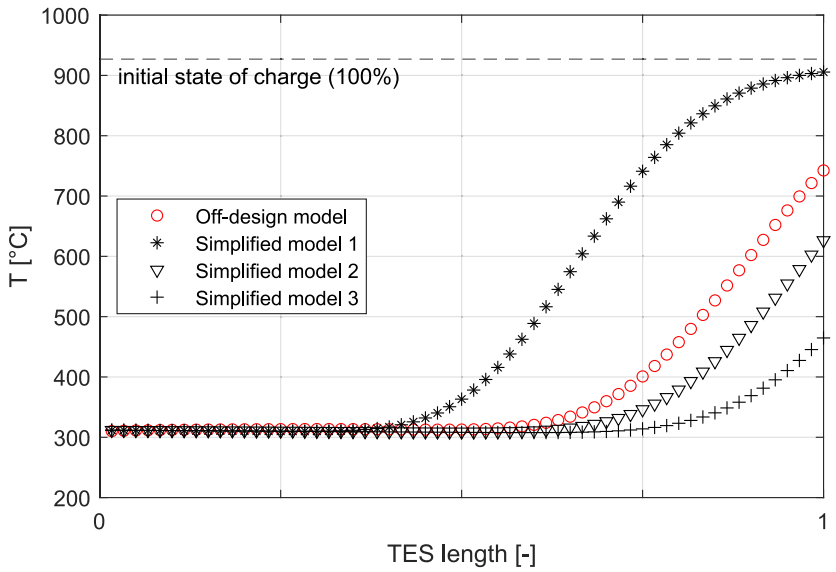

Fig. 10. State of charge of the TES after full discharge process: comparison between the comprehensive off-design model proposed in this work and different simplified models from literature.

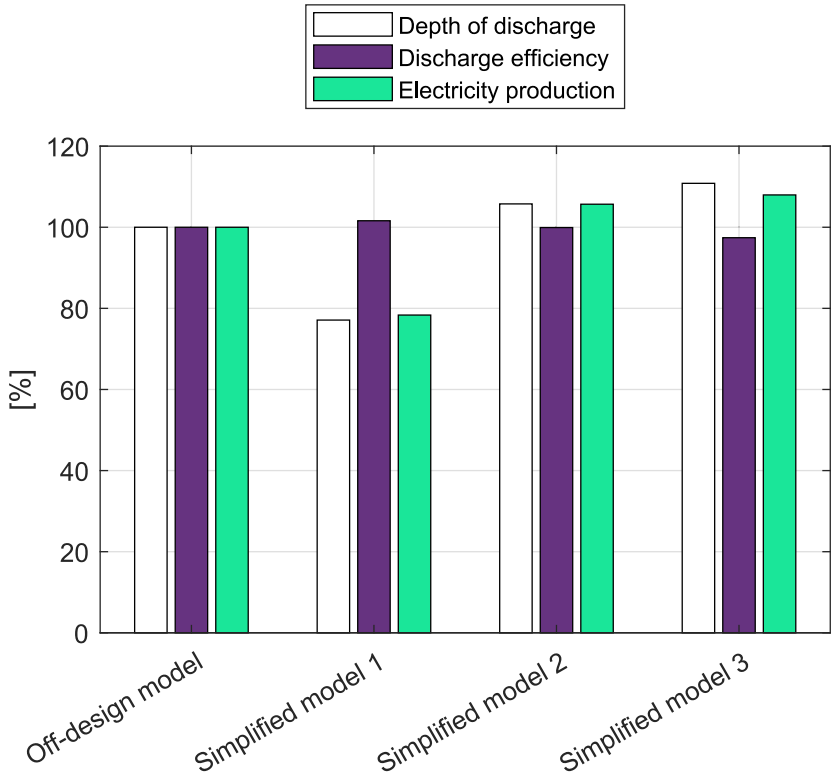

Fig. 11. Evaluation of depth of discharge, discharge efficiency and electricity production during a full discharge: percentage error using various simplified models from literature, with respect to the off-design model proposed in this work.

model of the plant has been built. The model takes into account the part-load behaviour of the turbomachinery with a zero-dimensional approach using performance maps. Although it includes a dynamic description of the Thermal Energy Storage, the model of the system calculates pseudo-steady-state points. In this way, the behaviour of the plant during a complete discharge can be studied, starting from an isothermal reservoir.

The results show that the temperature of the reservoir strongly affects the maximum discharge duration. With an increase in tank temperature, both the total discharge time and the nameplate power discharge time increase. However, the discharge duration can be tuned, according to the requirements of the grid, by regulating the output power of the system. The results also show that the number of layers for TES discretisation is not as relevant for the calculation of the performance of the whole system. Therefore, this parameter can be kept to the minimum possible to speed up the computation time without significantly affecting the model accuracy. The average efficiency of the delivery phase, for the selected working conditions, is equal to 27%. However, during discharge, the efficiency decreases from a maximum value of 29% to a minimum of 22%. The maximum depth of discharge

of the TES results in 64% due to the limited operating range of the turbomachinery. Comparison with simplified models from the literature shows that comprehensive off-design modelling is fundamental to predicting the maximum depth of discharge of Brayton-based Carnot batteries. In fact, using simplified models, the error ranges from 7% to 23%.

Future developments will involve the implementation of off-design characteristics of the fan, electric heater, and heat exchanger in the charging model. In this way, the round-trip efficiency can be defined and computed as well as the thermodynamic and economic performance of the full operation of the system. After that, the dynamic behaviour can be analysed and tailor-made management strategies developed based on grid needs.

Nomenclature

Abbreviations

CAES Compressed Air Energy Storage

CB Carnot Battery

EH Electric Heater

ES Energy Storage

FB Flow Batteries

HX Heat Exchanger

I-ESS Integrated Electricity Storage System

LAES Liquid Air Energy Storage

PHS Pumped Hydro Storage

PTES Pumped Thermal Energy Storage

RES Renewable Energy Storage

TES Thermal Energy Storage

TIT Turbine Inlet Temperature

VIGVs Variable Inlet Guide Vanes

Constants and variables

cp specific heat, J kg^{-1} K^{-1}

$\dot{m}$ mass flow rate, $kg\,s^{-1}$

N rotational speed

n number of layers

pr pressure ratio

T temperature

α_{IGV} Variable Inlet Guide Vanes position

β auxiliary coordinate of turbomachinery performance maps

η_{is} isentropic efficiency

Subscripts and superscripts

c compressor

t turbine

el electrical

th thermal

CRediT authorship contribution statement

Matteo Pecchini: Writing – review & editing, Writing – original draft, Validation, Methodology, Investigation, Formal analysis. **Simone Peccolo:** Writing – review & editing, Writing – original draft, Validation, Investigation. **Alberto Benato:** Writing – review & editing, Supervision, Methodology, Investigation, Conceptualization. **Francesco De Vanna:** Writing – review & editing, Validation, Investigation. **Anna Stoppato:** Writing – review & editing, Supervision, Methodology, Investigation, Conceptualization.

Declaration of competing interest

The authors declare that they have no known competing financial interests or personal relationships that could have appeared to influence the work reported in this paper.

Data availability

The data that has been used is confidential.

References

[1] IEA, Electricity market report 2023, 2023.
[2] IEA, Renewable energy market update - june 2023, 2023.
[3] Z. Dalala, M. Al-Omari, M. Al-Addous, M. Bdour, Y. Al-Khasawneh, M. Alkasrawi, Increased renewable energy penetration in national electrical grids constraints and solutions, Energy 246 (2022) 123361.
[4] K. Divya, J. Østergaard, Battery energy storage technology for power systems—An overview, Electr. Power Syst. Res. 79 (4) (2009) 511–520.
[5] G.L. Soloveichik, Battery technologies for large-scale stationary energy storage, Annu. Rev. Chem. Biomol. Eng. 2 (2011) 503–527.
[6] A. Benato, A. Stoppato, Pumped thermal electricity storage: a technology overview, Therm. Sci. Eng. Prog. 6 (2018) 301–315.
[7] B. Steffen, Prospects for pumped-hydro storage in Germany, Energy Policy 45 (2012) 420–429.
[8] J.P. Deane, B.Ó. Gallachóir, E. McKeogh, Techno-economic review of existing and new pumped hydro energy storage plant, Renew. Sustain. Energy Rev. 14 (4) (2010) 1293–1302.
[9] S. Rehman, L.M. Al-Hadhrami, M.M. Alam, Pumped hydro energy storage system: A technological review, Renew. Sustain. Energy Rev. 44 (2015) 586–598.
[10] E. Barbour, I.G. Wilson, J. Radcliffe, Y. Ding, Y. Li, A review of pumped hydro energy storage development in significant international electricity markets, Renew. Sustain. Energy Rev. 61 (2016) 421–432.
[11] G. Venkataramani, P. Parankusam, V. Ramalingam, J. Wang, A review on compressed air energy storage–a pathway for smart grid and polygeneration, Renew. Sustain. Energy Rev. 62 (2016) 895–907.
[12] J. Ke, W. He, M. Dooner, X. Luo, J. Wang, Compressed air energy storage system dynamic modelling and simulation, Compress. Air Energy Storage Types Syst. Appl. 184 (2021) 135.
[13] A. Vecchi, K. Knobloch, T. Liang, H. Kildahl, A. Sciacovelli, K. Engelbrecht, Y. Li, Y. Ding, Carnot battery development: A review on system performance, applications and commercial state-of-the-art, J. Energy Storage 55 (2022).
[14] A. Lampasi, V. Novotny, V. Basta, P. Smola, J. Spale, Review of carnot battery technology commercial development, 2022.
[15] O. Dumont, G.F. Frate, A. Pillai, S. Lecompte, V. Lemort, et al., Carnot battery technology: A state-of-the-art review, J. Energy Storage 32 (2020) 101756.
[16] T. Desrues, J. Ruer, P. Marty, J.-F. Fourmigué, A thermal energy storage process for large scale electric applications, Appl. Therm. Eng. 30 (5) (2010) 425–432.
[17] J.D. McTigue, A.J. White, C.N. Markides, Parametric studies and optimisation of pumped thermal electricity storage, Appl. Energy 137 (2015) 800–811.
[18] A. Benato, Performance and cost evaluation of an innovative pumped thermal electricity storage power system, Energy 138 (2017) 419–436.
[19] A. Benato, A. Stoppato, Energy and cost analysis of an air cycle used as prime mover of a thermal electricity storage, J. Energy Storage 17 (2018) 29–46.
[20] A. Benato, A. Stoppato, Integrated thermal electricity storage system: Energetic and cost performance, Energy Convers. Manage. 197 (2019) 111833.
[21] A. Benato, F. De Vanna, A. Stoppato, Levelling the photovoltaic power profile with the integrated energy storage system, Energies 15 (24) (2022) 9521.
[22] A. Benato, F. DE VANNA, E. Gallo, A. Stoppato, Thermal energy storage system integrating into a PV facility, in: Proceedings of ECOS 2022-35th International Conference on Efficiency, Cost, Optimization, Simulation and Environmental Impact of Energy Systems, 2022.

[23] A. Benato, M. Pecchini, F. DE VANNA, A. Stoppato, Off-design analysis of a TES-based electricity storage system, in: Proceedings of ECOS 2023-36th International Conference on Efficiency, Cost, Optimization, Simulation and Environmental Impact of Energy Systems, 2023.
[24] G.F. Frate, L. Paternostro, L. Ferrari, U. Desideri, Off-design of a pumped thermal energy storage based on closed brayton cycles, J. Eng. Gas Turbines Power 144 (2) (2022).
[25] G.F. Frate, A. Baccioli, L. Bernardini, L. Ferrari, Assessment of the off-design performance of a solar thermally-integrated pumped-thermal energy storage, Renew. Energy 201 (2022) 636–650.
[26] A. Benato, F. De Vanna, E. Gallo, A. Stoppato, G. Cavazzini, TES-PD: A fast and reliable numerical model to predict the performance of thermal reservoir for electricity energy storage units, Fluids 6 (7) (2021) 256.
[27] M. Abarr, B. Geels, J. Hertzberg, L.D. Montoya, Pumped thermal energy storage and bottoming system part a: Concept and model, Energy 120 (2017) 320–331.
[28] M. Abarr, J. Hertzberg, L.D. Montoya, Pumped thermal energy storage and bottoming system part b: sensitivity analysis and baseline performance, Energy 119 (2017) 601–611.
[29] Y. Ge, Y. Zhao, C. Zhao, Transient simulation and thermodynamic analysis of pumped thermal electricity storage based on packed-bed latent heat/cold stores, Renew. Energy 174 (2021) 939–951.
[30] L. Wang, X. Lin, L. Chai, L. Peng, D. Yu, H. Chen, Cyclic transient behavior of the joule–brayton based pumped heat electricity storage: Modeling and analysis, Renew. Sustain. Energy Rev. 111 (2019) 523–534.
[31] H. Zhang, L. Wang, X. Lin, H. Chen, Operating mode of brayton-cycle-based pumped thermal electricity storage system: Constant compression ratio or constant rotational speed?, Appl. Energy 343 (2023) 121107.
[32] J. Kurzke, Gasturb 12: A program to calculate design and off-design performance of gas turbines. users manual, GasTurb, Aachen, Germany, 2012.
[33] M.B. Hashmi, T.A. Lemma, Z.A. Abdul Karim, Investigation of the combined effect of variable inlet guide vane drift, fouling, and inlet air cooling on gas turbine performance, Entropy 21 (12) (2019).
[34] D.E. Muir, H.I.H. Saravanamuttoo, D.J. Marshall, Health Monitoring of Variable Geometry Gas Turbines for the Canadian Navy, J. Eng. Gas Turbines Power (ISSN: 0742-4795) 111 (2) (1989) 244–250.
[35] A. Paul, F. Holy, M. Textor, S. Lechner, High temperature sensible thermal energy storage as a crucial element of carnot batteries: Overall classification and technical review based on parameters and key figures, J. Energy Storage 56 (2022).
[36] A. Razak, Industrial gas turbines: performance and operability, Elsevier, 2007.
[37] M.J. Powell, A fortran subroutine for solving systems of nonlinear algebraic equations, in: Tech. rep., Atomic Energy Research Establishment, Harwell, England (United Kingdom), 1968.
[38] P.P. Walsh, P. Fletcher, Gas turbine performance, John Wiley & Sons, 2004.
[39] S. Li, Z. Li, S. Li, Improved Method for Gas-Turbine Off-Design Performance Adaptation Based on Field Data, J. Eng. Gas Turbines Power 142 (4) (2020) 041001.